Influence of carbon, manganese and nickel on microstructure and properties of strong steel weld metals
Part 1 – Effect of nickel content

E. Keehan*[1], L. Karlsson[2] and H.-O. Andrén[3]

The effects of increasing the nickel content from 3 to 7 or 9 wt-% were investigated in high strength steel weld metals with 2 wt-% manganese. Nickel additions were beneficial to strength but detrimental to impact toughness. Significant segregation of nickel and manganese to interdendritic regions was observed at the two higher nickel contents. In these weld metals a mainly martensitic microstructure developed at interdendritic regions, whereas bainite was found at dendrite core regions. The microstructural inhomogeneity was due to segregation and the accompanying stabilisation of austenite in solute enriched regions to lower transformation temperatures. With 3 wt-% nickel the microstructure was found to be more homogeneous, with mainly bainite forming. The decrease in impact toughness with increasing nickel content was mainly attributed to the formation of coarse grained coalesced bainite.

Keywords: Nickel, High strength steel, Weld metal, Manganese, Strength, Impact toughness, Segregation, Martensite, Bainite, Microstructure, Austenite, Transformation temperature, Coalesced bainite

Introduction

High strength steel with yield strength greater than 690 MPa (100 ksi) has been welded on a limited scale and with many precautions since the 1960s. Using mainly gas tungsten arc welding and tightly controlled conditions it proved possible to produce weld metals with both good strength and good toughness. These weld metals have had limited use, primarily owing to economic factors and lack of flexibility. In recent years there has been a growing demand for high strength steels in such fields as construction, offshore, and heavy engineering.[1] Given the very nature of these applications, welding must be flexible and economical and mechanical properties must be insensitive to the welding procedure. Shielded metal arc welding (SMAW), flux cored arc welding, and submerged arc welding offer the flexibility and productivity required. However, with these methods toughness becomes problematic as strength levels increase.

Focusing on the SMAW method, current compositions utilised in high strength consumables are usually in the range 0·04–0·08C, 1–2Mn, 0·2–0·5Si, and 1–3Ni (all compositions are in wt-% throughout unless stated otherwise) along with minor additions of chromium, molybdenum, and sometimes copper.[1–3] From a review of literature on the role and effects of the individual alloying elements, nickel drew attention since it was reported to influence the stacking fault energy in such a manner that it becomes easier for ferrite to undergo plastic deformation at low temperartures.[4] In addition it is known to solid solution harden and to increase the hardenability, both promoting higher strength.[5] At higher concentrations it leads to an increase in the retained austenite content of the final microstructure.

In contrast, neural network modelling predicted that at manganese contents greater than 1·5%, nickel additions lead to losses in toughness, whereas below 1·5% manganese, the nickel can improve toughness.[6] Remarkably, when experimental weld metals were produced and the mechanical properties compared, it was found that the predictions were correct.[6] Weld metals reported in the literature, with nickel contents up to 7% and various manganese contents, were also found to be consistent with the predictions.[7,8]

When investigations of the 7 and 9% nickel weld metals were carried out using light optical microscopy (LOM), the microstructure was found to have fine scale morphology typical of martensite or bainite along with a novel constituent with large grain size.[9] Further studies using high resolution techniques on the 7% nickel weld metal revealed a lath like microstructure of martensite at interdendritic regions along with mainly a mixture of upper, lower, and a novel coarse grained bainite in dendrite core regions. The novel constituent was

[1]ESAB AB, PO Box 8004, SE–402 77 Gothenburg, Sweden. Work carried out in the Department of Applied Physics, Chalmers University of Technology, Kemigården 1, Fysikgränd 3, SE–412 96 Gothenburg, Sweden
[2]ESAB AB, PO Box 8004, SE–402 77 Gothenburg, Sweden
[3]Department of Applied Physics, Chalmers University of Technology, Kemigården 1, Fysikgränd 3, SE–412 96 Gothenburg, Sweden

*Corresponding author, email enda.keehan@esab.se

Published by Maney on behalf of the Institute
Received 7 April 2005; accepted 22 June 2005
DOI 10.1179/174329306X77830

revealed to be coalesced bainite with an unusually large size.[10] The present paper is the first in a series of three dealing with the effects of nickel, manganese,[11] and carbon[12] on high strength steel weld metals. In the present work, a comparison is made of the microstructure and properties of 7 and 9% nickel weld metals with those of a 3Ni–2Mn–0·5Cr–0·6Mo–0·05C commercial electrode (ESAB OK 75·78).

Experimental procedures

Welded joints were made according to ISO 2560[13] using 20 mm plates with a backing plate. The joints were buttered to limit dilution before the deposition of the experimental weld metals, which took place in 33 cm runs with two runs per layer and three on the top layer. Welding parameters and chemical compositions are presented in Table 1. It was decided to label the experimental weld metals 7–2L250 and 9–2L250, where 7 or 9 is the nickel content and 2 the manganese content (both wt-%), L indicates low carbon (0·03 wt-%), and 250 denotes the interpass temperature in °C.

For Charpy testing, transverse specimens were machined having dimensions of $10 \times 10 \times 55$ mm, notched perpendicular to the welding direction in the weld metal centre. Two or three specimens were tested at each temperature. Tensile specimens were machined longitudinally from the weld deposits with a specimen diameter of 10 mm and a gauge length of 70 mm. Charpy impact testing and tensile testing were performed in compliance with standard EN 10045–1.[15]

Specimens for metallographic analysis from the weld metal cross-section, perpendicular to the welding direction, were mounted in bakelite, wet ground, and polished to 1 μm diamond grain size. Polished samples were examined using scanning electron microscopy and specimens etched using 2% nital were studied using both LOM and field emission gun scanning electron microscopy (FEGSEM). A Leitz Aristomet LOM, a Philips XL30 SEM, and a Leo Ultra 55 FEGSEM were used in these examinations.

For transmission electron microscopy (TEM) studies, 3 mm disc shape specimens perpendicular to the welding direction were wet ground to between 50 and 80 μm in thickness. The discs were then jet electropolished at −35°C using 10% perchloric acid in methanol. After electropolishing, the samples (which contained a small hole with thin areas around it) were further thinned by ion beam milling for a few minutes at a low angle using a Gatan Precision Ion Polishing System. These specimens were examined with a Jeol 2000 FX TEM and a Philips CM 200 TEM.

Hollow and solid cylindrical dilatometry specimens were machined from the centre of the welded joint. Hollow specimens with an outer diameter of 4·9 mm, inner diameter of 3·5 mm, and length of 12·5 mm were used for measurements with cooling rates greater than 50 K s^{-1} whereas solid specimens with 3 mm diameter and 10 mm length were used for lower cooling rates. All specimens were analysed using a Theta Dilatronic III dilatometer to record phase transformation temperatures. The specimens were heated to 1000°C at a rate of 25 K s^{-1}, held for 5 min, and then cooled at different rates to room temperature. Individual samples were used for each cooling rate.

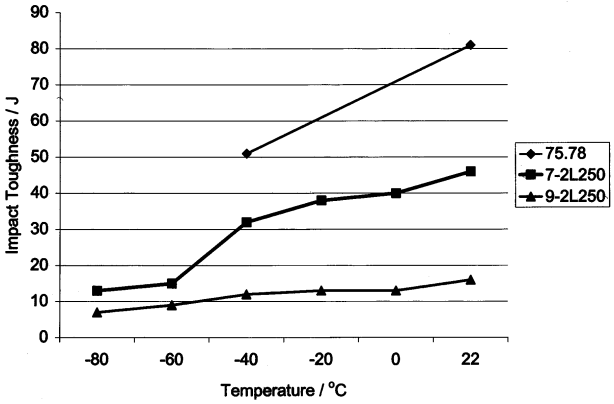

1 Charpy V notch impact toughness as function of temperature for weld metals

Results

Mechanical properties

It was found that nickel strengthens the alloy but reduces toughness, as predicted by the neural network modelling. Figure 1 shows that OK 75·78 with the lowest nickel content (3%) had the greatest impact toughness both at room temperature and at −40°C (81 and 51 J, respectively). A progressive loss of toughness was experienced as the nickel content was increased to 7 and then 9%. For the 9%Ni weld metal only 12 J was recorded at −40°C and 16 J at room temperature. In Table 2 it can be seen that nickel additions had a positive effect on strength. Examining first OK 75·78 with 3%Ni, a value of 756 MPa was recorded for yield strength and 945 MPa for ultimate tensile strength. The best tensile results were achieved for the 9%Ni weld metal, where a yield strength of 848 MPa and a tensile strength of 1051 MPa were recorded. Also, it should be noted that both the higher nickel alloys have slightly lower carbon content than OK 75·78.

Microstructure – last bead

The microstructure of OK 75·78 has previously been characterised; it consists of a mixture of martensite and bainite with the percentage of each directly related to the welding parameters.[16,17] Given this information, it was decided for the purpose of completeness to characterise the microstructure obtained for the given welding parameters using LOM and FEGSEM.

Table 1 Welding parameters and chemical composition (wt-%, except where indicated)

Weld metal	*E*, kJ mm^{-1}	IPT, °C	$t_{8/5}$, s	C*	Si	Mn	P	S*	Cr	Mo	Ni	Cu	O, ppm*	N, ppm*
OK 75·78	1·4	250	13	0·054	0·26	2·05	0·009	0·011	0·42	0·6	3·14	0·01	300	130
7–2L250	1·2	250	12	0·032	0·25	2·02	0·011	0·008	0·47	0·63	7·23	0·03	380	250
9–2L250	1·2	250	11	0·031	0·27	2·11	0·011	0·008	0·48	0·64	9·23	0·03	340	260

E energy input; IPT interpass temperature; $t_{8/5}$ estimated cooling time between 800 and 500°C calculated from WeldCalc.[14]
*Elements analysed using Leco Combustion equipment.

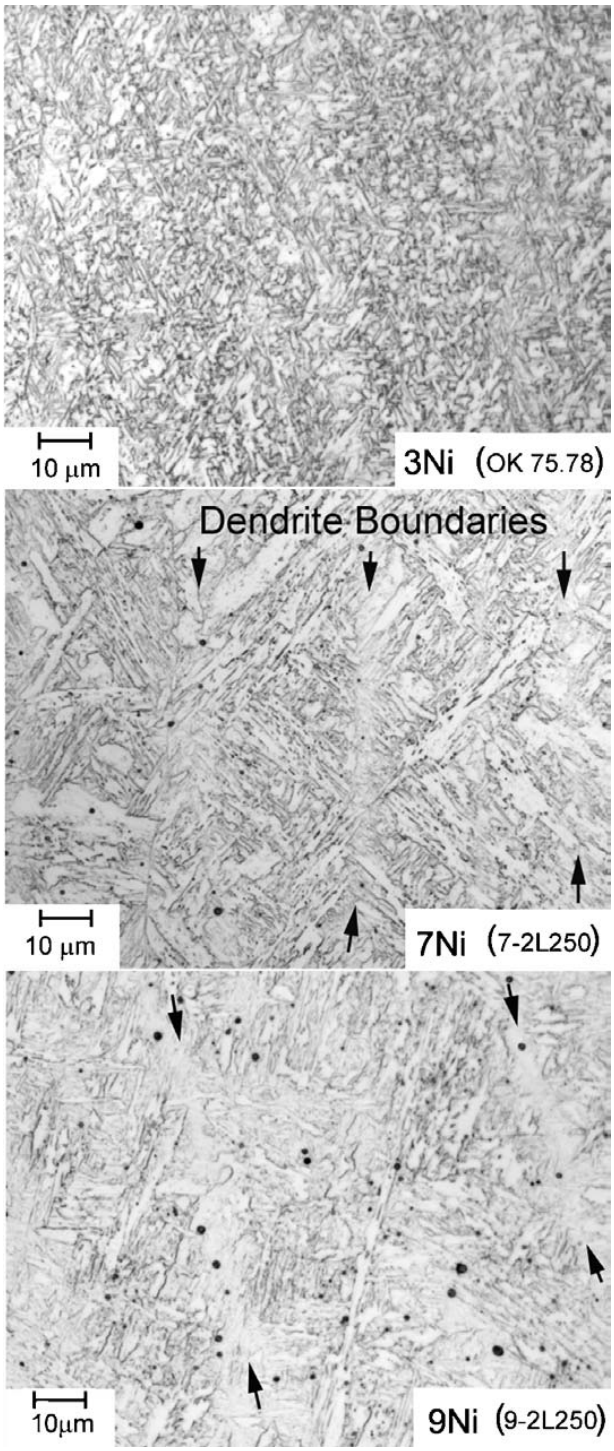

2 Microstructure of last bead of weld deposited with commercial electrode OK 75·78 and experimental weld metals 7–2L250 and 9–2L250 (LOM)

Microstructural investigations were first carried out on the as deposited last bead. Figure 2 shows LOM images from the three weld metals. In the experimental weld metals traces of the former dendritic structure that developed during solidification could be clearly seen. In work presented elsewhere this was explained on the basis that the experimental weld metals with greater nickel content solidify as austenite whereas OK 75·78 solidifies primarily as δ ferrite.[16] Overall it was concluded that a fine scale microstructure developed which was thought to be a mixture of martensite and bainite and characterisation tools with higher resolution were required for a complete interpretation.

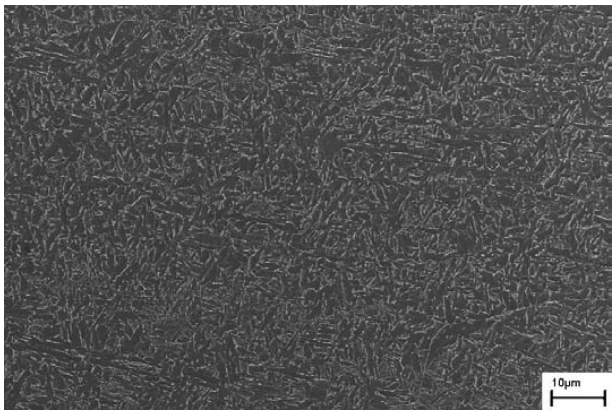

3 Overview of microstructure in last bead of OK 75·78 weld metal (FEGSEM)

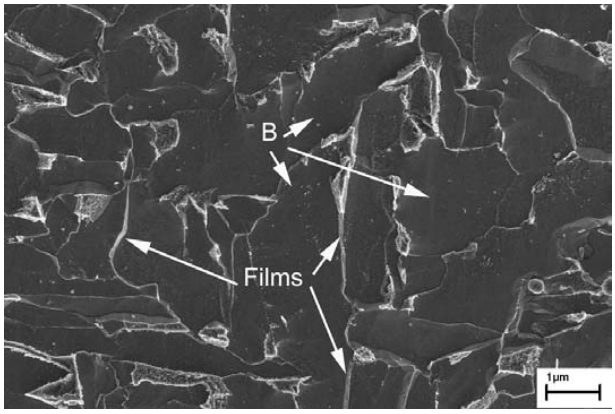

4 FEGSEM image confirming that microstructure is mainly bainitic (B) in last bead of OK 75·78 weld metal: films are also observed at bainitic ferrite boundaries

Investigations with FEGSEM were found to be very revealing. Micrographs from OK 75·78 weld metal are presented in Figs. 3–5. An overview of the microstructure is presented in Fig. 3 and from investigations at higher magnification (Figs. 4 and 5) it was found that the microstructure was mainly bainitic. In Fig. 4 it can be observed that films developed at the bainitic ferrite plate boundaries. In Fig. 5 at very high magnification, precipitates were also found within some of the plates.

Figures 6–9 show FEGSEM images from the experimental weld metals. It was found that these weld metals

Table 2 Tensile properties of weld metals

Weld metal	Yield strength (YS), MPa	Ultimate tensile strength (UTS), MPa	YS/UTS	A_5, %
OK 75·78	756	945	0·8	19·4
7–2L250	795	1006	0·79	14·8
9–2L250	848	1051	0·81	13·1

A_5 elongation.

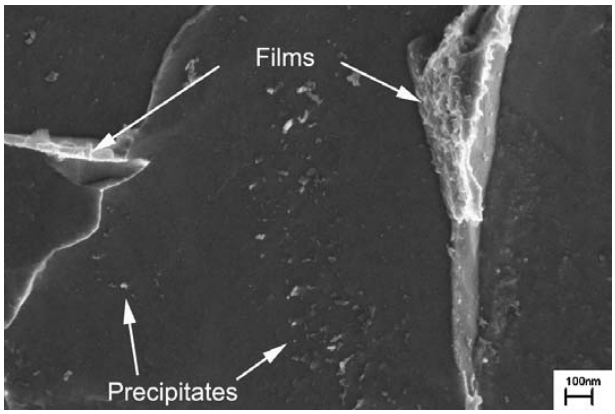

5 High magnification FEGSEM image, showing precipitates within bainitic ferrite and films at boundaries in last bead of OK 75·78 weld metal

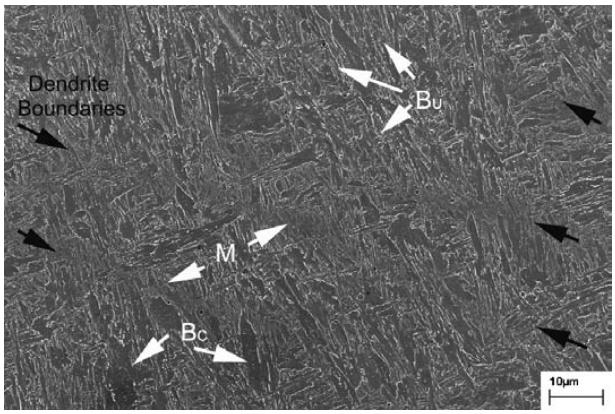

6 Last bead in 7–2L250 (FEGSEM), containing mixture of martensite (M), coalesced bainite (B_C), and upper bainite (B_U)

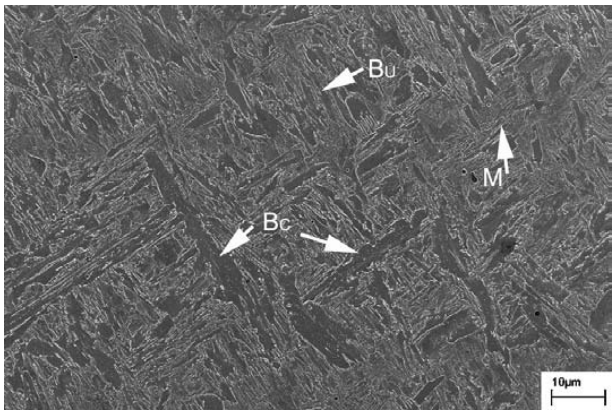

7 Last bead in 9–2L250, showing mainly martensite at interdendritic regions along with coalesced lower bainite and upper bainite at dendrite core regions (FEGSEM)

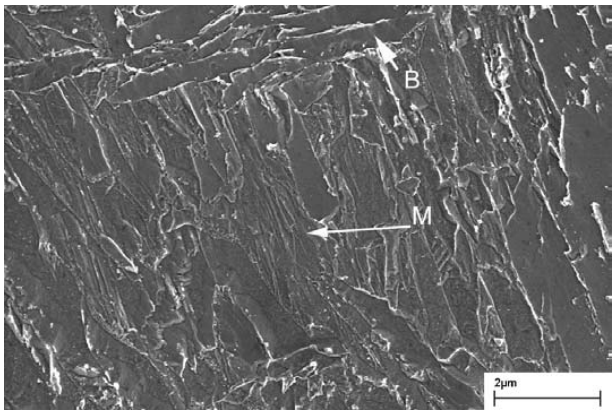

8 Interdendritic region in last bead of 7–2L250 at high magnification, showing mainly martensite at former dendrite boundary: upper bainite, characterised by absence of intragranular precipitates, can also be seen within image (FEGSEM)

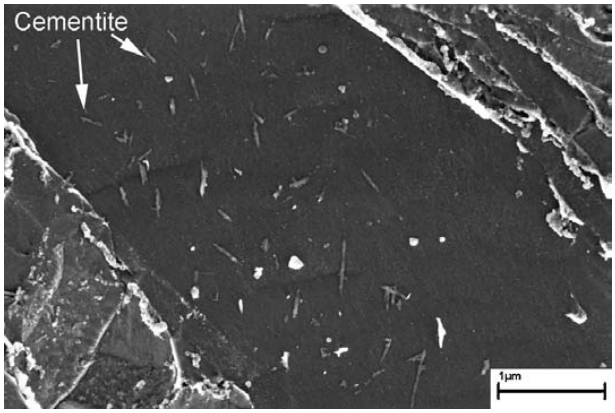

9 Higher magnification image showing precipitation within bainitic ferrite plate in 9–2L250 (FEGSEM)

were similar and there were noticeable differences from the OK 75·78 weld metal. Using FEGSEM it was again possible to see the former dendrite boundaries that developed during solidification. Low magnification micrographs giving overviews of the microstructure in both weld metals are shown in Figs. 6 and 7. In both micrographs it can be seen that a finer morphology formed at the interdendritic regions. Figure 8 shows a representative micrograph of a former interdendritic region at higher magnification in weld metal 7–2L250. In this region the microstructure was mainly martensite. Some distance from the dendrite boundary, upper bainite can also be observed in the micrograph. In dendrite core regions, large grains several micrometres in size can be observed (Figs. 6 and 7). In previous work[10] on 7–2L250, these large grains were characterised to be a special form of bainite with a large grain size, forming when the bainite and martensite start temperatures are very close. This type of bainite is known as coalesced bainite. Figure 9 shows coalesced bainite in weld metal 9–2L250 at high magnification. It was observed that precipitates formed within the bainitic ferrite. Many of these precipitates are identified as cementite since precipitates of similar size and morphology were characterised via TEM in previous work on 7–2L250.[10]

Elemental distribution

Investigations on polished samples using SEM in the backscattered mode gave a clear contrast between the dendrite boundary and core regions in the last bead of the experimental weld metals. Line scans were made across the dendrites using EDX and the results are plotted in Fig. 10. It can be seen that the concentrations follow a wavelike pattern, with segregation of manganese and nickel reaching a maximum concentration at

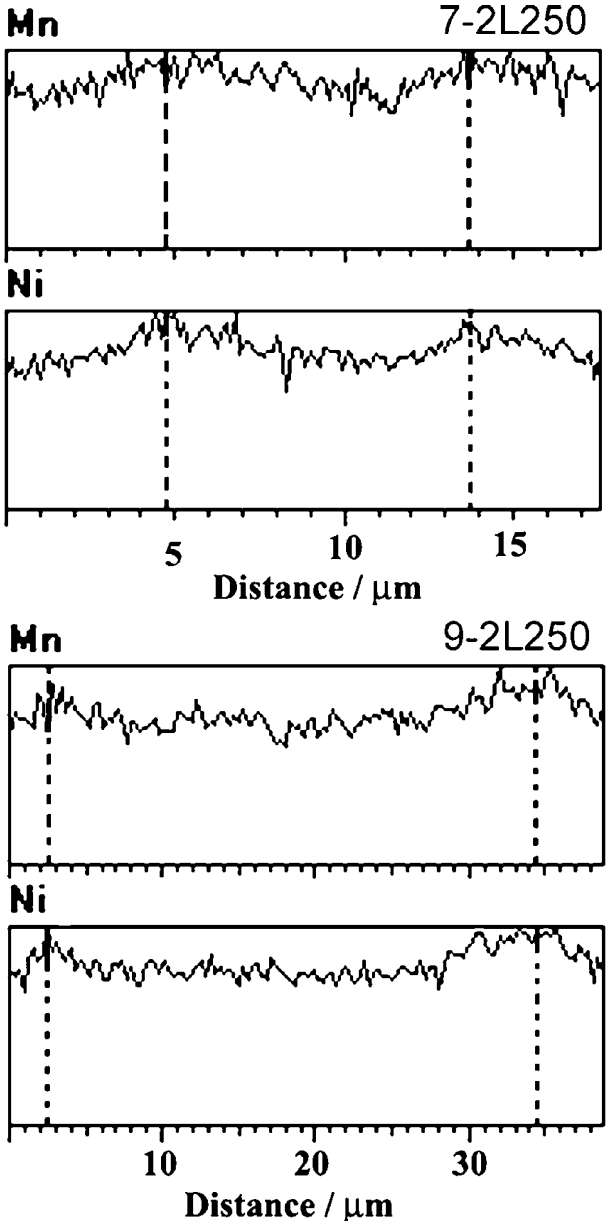

10 Line scans (EDX) across dendrites in last bead of 7–2L250 and 9–2L250, showing segregation of nickel and manganese to interdendritic regions (indicated by broken lines): *y* axis shows relative intensity measured for given element

the dendrite boundaries. The degree of segregation was quantified using spot analysis, and between five and ten examinations were carried out in both the dendrite core regions and the interdendritic regions. The results presented in Table 3 are the average values recorded in each region. Despite the overestimation of manganese, the results allow a clear comparison and a clear estimation of the degree of segregation between the dendrite boundaries and centres. Weld metal 9–2L250 showed the greatest difference between the two regions, with a difference of 1·15 wt-% for manganese and 2·6 wt-% for nickel.

Table 3 Average compositions (wt-%) at dendrite boundary regions and dendrite centre in last bead, obtained using EDX spot analysis

Weld metal	Region	Mn	Ni
7–2L250	Boundary	3·10	8·18
7–2L250	Centre	2·35	6·30
7–2L250	Difference	0·75	1·88
9–2L250	Boundary	3·20	10·30
9–2L250	Centre	2·05	7·70
9–2L250	Difference	1·15	2·60

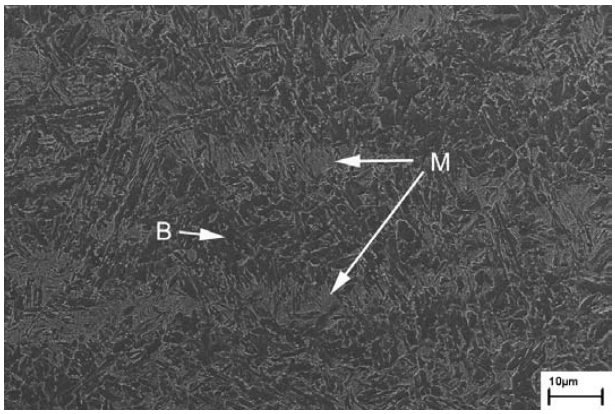

11 Overview showing microstructure in centre of reheated OK 75·78 weld bead: tempered martensite is mainly found at dendrite boundary regions and bainite in centre of dendrites (FEGSEM)

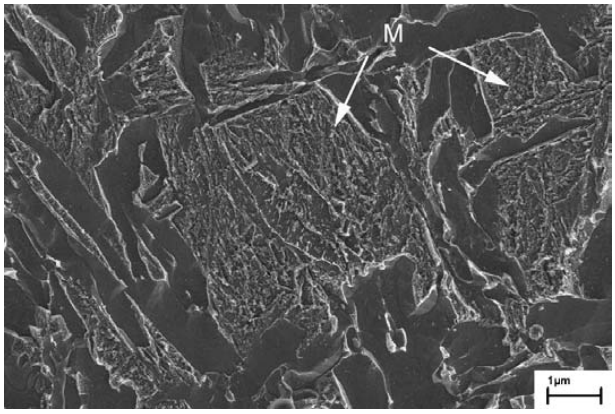

12 Large amounts of tempered martensite in interdendritic region in centre of reheated OK 75·78 weld bead, observed using FEGSEM

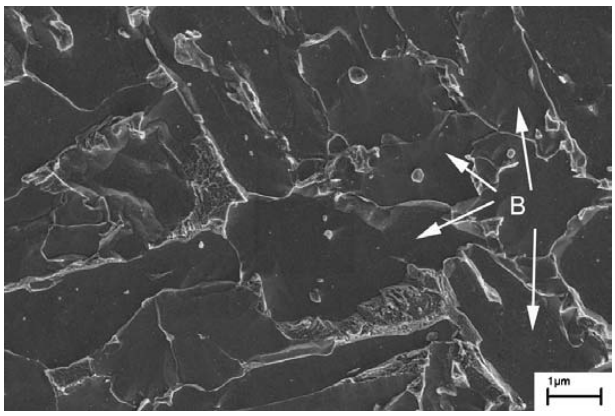

13 Centre of reheated bead in OK 75·78, showing mainly tempered bainite (FEGSEM)

Microstructure – reheated beads

Figures 11–13 show FEGSEM images from the centre of a reheated bead in OK 75·78 weld metal. After

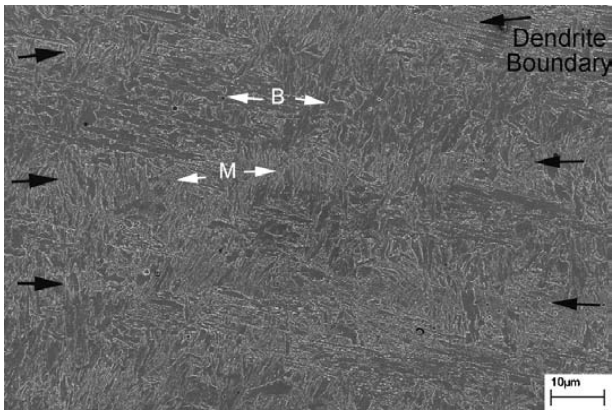

14 Overview showing centre of reheated bead in 7–2L250: tempered martensite is mainly found at dendrite boundary regions and tempered bainite in centre of dendrites (FEGSEM)

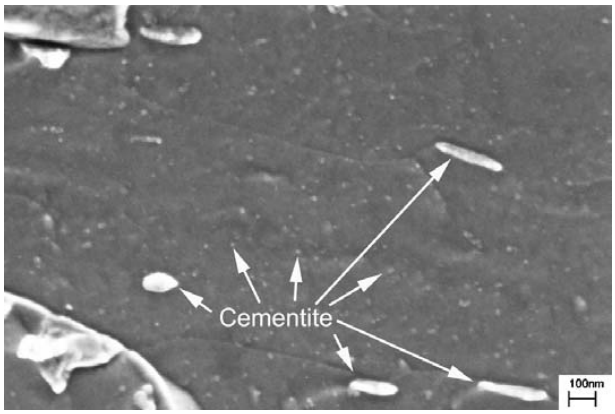

16 Large and very small cementite precipitates in bainitic ferrite after reheating in dendrite core region of 7–2L250 (FEGSEM): interpretations were based on TEM investigations

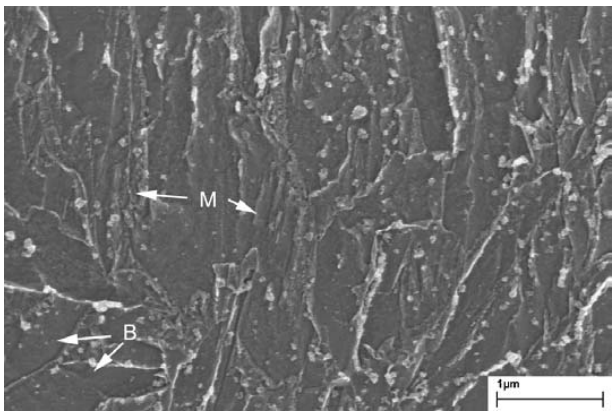

15 High magnification FEGSEM image of interdendritic region, showing general appearance of mainly tempered martensite in reheated weld bead of 7–2L250 – some tempered bainite can also be seen

reheating, traces of the former dendrite structure could be observed to a limited degree in Fig. 11. A large amount of tempered martensite was found at the former interdendritic regions with tempered bainite at dendrite core regions. The morphology of the individual constituents is shown at higher magnification in Figs. 12 and 13.

The reheated microstructure of the experimental weld metals was also examined using FEGSEM and some micrographs are presented in Figs. 14–16. An overview of the microstructure in 7–2L250 is shown in Fig. 14. It was generally found that the microstructure consisted of tempered martensite in dendrite boundary regions and tempered bainite in the centre of the dendrites (Fig. 15). The location of the cementite within the microstructure shown in Fig. 16 was interpreted based on understanding obtained from TEM investigations.[10]

Investigations with TEM were carried out on reheated beads of both 7–2L250 and 9–2L250. Results from 9–2L250 are presented in Figs. 17 and 18, and (limited) results from 7–2L250 are presented in previous work.[10] Figure 17 shows bright and dark field images with a corresponding selected area diffraction pattern from weld metal 9–2L250. The reflections in the diffraction pattern were found to correspond to ferrite and cementite.[18–20] When a cementite reflection was selected to form a dark field image it was seen that very small

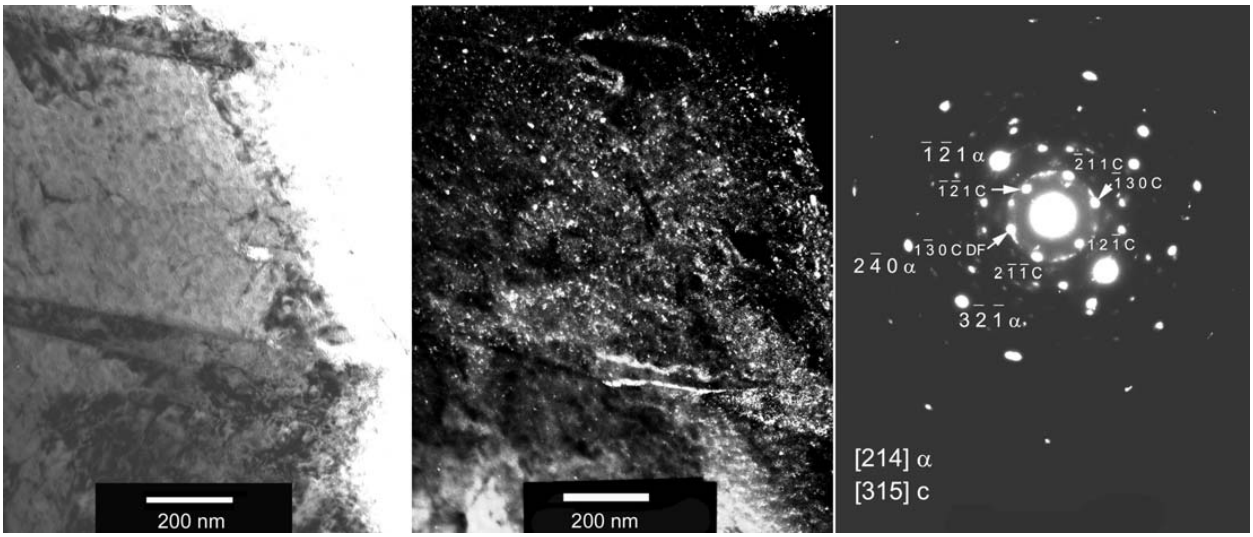

17 Bright and dark field TEM images with corresponding selected area diffraction pattern of cementite obtained from centre of reheated bead in weld metal 9–2L250: dark field image was formed using [130] C (cementite) reflection in corresponding diffraction pattern

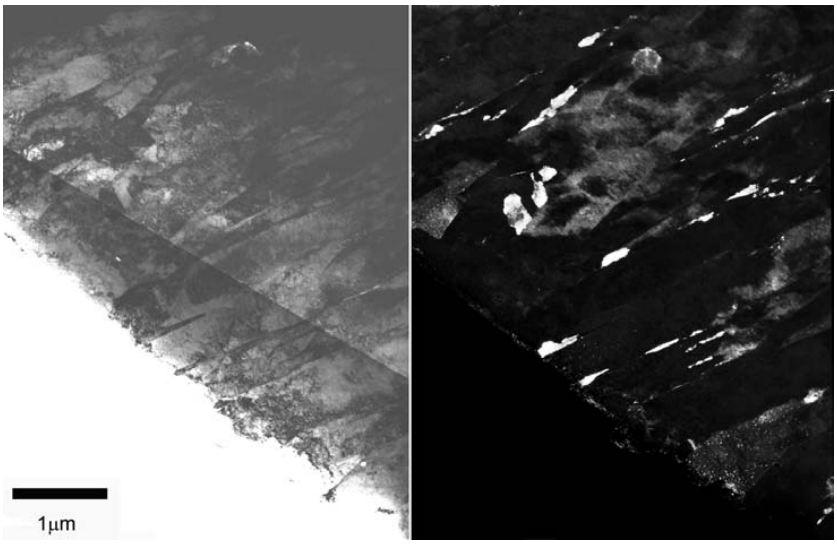

18 Bright and dark field TEM images of cementite at lath boundaries in centre of reheated bead in weld metal 9–2L250 (note adjustment of contrast in top of bright field image to allow grains in specimen to be observed, resulting in diagonal line in image)

precipitates (<15 nm) in the bright field image were illuminated. A low magnification bright and dark field image of the same area, showing cementite both at plate boundaries and within plates, is presented in Fig. 18.

Dilatometry

Phase transformation temperatures were measured using dilatometry. It was found that Ac_1 and Ac_3 were at 665 and 720°C respectively for 9–2L250 when samples were heated at a rate of 25 K s^{-1} from room temperature. These can be compared with 690 and 740°C for Ac_1 and Ac_3 for 7–2L250.

Austenite began transformation in the region of 365°C when cooled at a rate of approximately 30 K s^{-1}, as well as at 1 K s^{-1}, for weld metal 9–2L250. With 7% nickel, transformation temperatures were slightly higher, with 373°C and 390°C being recorded at cooling rates of 25 and 1 K s^{-1}, respectively.

Discussion

In the present work it was found that the effect of nickel additions was positive for strength but negative for toughness at a manganese content of 2%. The nickel content, its interaction with other alloying elements, segregation, and its effect on transformation temperature all play a major role. Ultimately it determines the phases and constituents that develop during solidification and cooling, which in turn govern the mechanical properties.

From microscopy it was found that the overall microstructure was very fine in the 7 and 9%Ni weld metals. Using a combination of FEGSEM and TEM a mixture of bainite, martensite, and films of retained austenite[10] was observed. It is concluded from thermodynamic modelling[9] that these weld metals solidify as austenite, resulting in significant segregation. In both weld metals, segregation of nickel and manganese to interdendritic regions was observed and quantified using EDX analysis (Table 3). These local differences in alloying content are thought to cause the microstructural differences across the dendrites. Dilatometry measurements showed that both nickel and manganese[11] stabilise austenite to lower transformation temperatures. In agreement with this, coalesced bainite and upper bainite were mainly found in dendrite core regions whereas martensite was found predominantly at interdendritic regions (Figs. 6 and 7).

In regions reheated owing to multiple weld passes the microstructure consisted of a mixture of tempered bainite and tempered martensite (Figs. 14 and 15). Overall there was no remarkable difference between the microstructures of 7–2L250 and 9–2L250. Coarsening and spheroidising of cementite was seen and very numerous small precipitates were also found to form. These precipitates most probably developed from the carbon dissolved on reheating to temperatures close to or above Ac_1.

In contrast to the experimental weld metals, OK 75·78 was found to be mainly bainitic in nature in the as deposited last bead. This weld metal solidifies predominantly as δ ferrite[17] and as a result segregation was not as pronounced. Precipitates were observed within the bainitic ferrite and films were found at the boundaries (Fig. 5). Overall the microstructure was more homogeneous in its morphology (Figs. 2 and 3) and there was the notable absence of coalesced bainite. In reheated regions, OK 75·78 had many similarities to the experimental weld metals but there were also some differences. Similarly to the experimental weld metals, OK 75·78 formed some martensite at interdendritic regions and bainite within the dendrites. However, it was noted that the grain size in these regions was finer than in the experimental weld metals.

The loss of toughness experienced with nickel additions can be attributed mainly to the larger effective grain size developed within the microstructure, which is expected to offer little resistance to cleavage crack propagation. Increasing nickel content stabilised austenite to lower transformation temperatures and promoted the formation of coarse grained coalesced bainite and martensite. The extra strength is most probably due to the combination of solid solution hardening attained from nickel and the greater amounts of martensite present within the microstructure.

Conclusions

Nickel additions stabilised austenite to lower transformation temperatures. Greater amounts of martensite and coalesced bainite were formed as nickel content increased. Segregation of nickel and manganese to interdendritic regions leads to greater amounts of martensite forming at interdendritic regions and more bainite at dendrite core regions.

For the level of manganese present, nickel increased the strength but reduced the toughness of the weld metal. The strength was increased by solid solution hardening due to nickel additions and greater amounts of martensite. The decrease in toughness with nickel additions was mainly due to the formation of coarse grained coalesced bainite.

Acknowledgements

Professor L.-E. Svensson of Chalmers University of Technology and Professor H. K. D. H. Bhadeshia of the University of Cambridge are thanked for fruitful discussions. Mr P. Lindström of Sandvik Materials Technology is thanked for help with dilatometry experiments. ESAB AB is thanked for the production of experimental weld metals, permission to publish results, and financial support. The Knowledge foundation of Sweden is thanked for additional financial support.

Reference

1. D. J. Widgery, L. Karlsson, M. Murugananth and E. Keehan: 'Approaches to the development of high strength weld metals', Proc. 2nd Int. Symp. on 'High strength steel', Verdal, Norway, April 2002, SINTEF Materials Technology.
2. W. Wang and S. Liu: *Weld. J.*, 2002, **81**, (7), 132s.
3. D. P. Fairchild, M. L. Macia, N. V. Bangaru and J. Y. Koo: Proc. 13th Int. Offshore and Polar Eng. Conf., Honolulu, Hawaii, USA, May 2003, p. 26.
4. L.-E. Svensson: 'Control of microstructure and properties in steel arc welds', 69; 1994, Boca Raton, FL, USA, CRC Press.
5. S. Lampman (tech. ed.): in 'Weld integrity and performance', 218; 1997, Materials Park, OH, USA, ASM International.
6. M. Murugananth, H. K. D. H. Bhadeshia, E. Keehan, H. O. Andrén and L. Karlsson: 'Strong and tough ferritic steel welds', in 'Mathematical modelling of weld phenomena 6', (ed. H. Cerjak), 205–230; 2002, Abington, Woodhead.
7. Y. Kang, H. J. Kim and S. K. Hwang: *ISIJ Int.*, December 2000, **40**, 1237.
8. Z. Zhang and R. A. Farrar: *Weld. J.*, 1997, **76**, (5), 183s–196s.
9. E. Keehan: PhD thesis, Paper 7, Chalmers University of Technology, Gothenburg, Sweden, 2004.
10. E. Keehan: PhD thesis, Paper 3, Chalmers University of Technology, Gothenburg, Sweden, 2004.
11. E. Keehan, L. Karlsson, H. O. Andrén and H. K. D. H. Bhadeshia: *Sci. Technol. Weld. Joining*, 2006, **11**, (1), 9–18.
12. E. Keehan, L. Karlsson, H. O. Andrén and H. K. D. H. Bhadeshia: *Sci. Technol. Weld. Joining*, 2006, **11**, (1), 19–24.
13. 'Welding consumables – covered electrodes for manual metal arc welding of non alloy and fine grain steels – classification', DIN Standard ISO 2560 : 2002.
14. 'WeldCalc' software, Version 1.0.0, SSAB, Oxelösund, Sweden, 1998–1999.
15. 'Charpy impact test on metallic materials; part 1: test method', DIN Standard EN 10045–1 : 1991.
16. M. Lord: *Weld. World*, 1998, **41**, 452.
17. M. Lord: 'Design and modelling of ultra-high strength steel weld deposits', PhD thesis, University of Cambridge, Cambridge, UK, 1999.
18. K. W. Andrews, D. J. Dyson and S. R. Keown: 'Interpretation of electron diffraction patterns', 2nd edn; 1971, London, Adam Hilger.
19. J. W. Edington: 'Practical electron microscopy in material science', 118; 1975, London, The Macmillan Press.
20. Internet http://cimesg1.epfl.ch/CIOL/ems.html, Centre Interdisciplinaire de Microscopie Electronique, Ecole Polytechnique Fédérale de Lausanne, Lausanne, France.